

CanvasMAR: Improving Masked Autoregressive Video Prediction With Canvas

Zian Li^{1,2} and Muhan Zhang^{1,3*}

¹ Institute for Artificial Intelligence, Peking University, Beijing, China

² School of Intelligence Science and Technology, Peking University, Beijing, China

³ State Key Laboratory of General Artificial Intelligence, Peking University, Beijing, China

zian@stu.pku.edu.cn, muhan@pku.edu.cn

Abstract. Masked autoregressive models (MAR) have emerged as a powerful paradigm for image and video generation, combining the flexibility of masked modeling with the expressiveness of continuous tokenizers. However, when sampling individual frames, video MAR models often produce highly distorted outputs due to the lack of a structured global prior, especially when using only a few sampling steps. To address this, we propose **CanvasMAR**, a novel autoregressive video prediction model that predicts high-fidelity frames with few sampling steps by introducing a canvas—a blurred, global one-step prediction of the next frame that serves as a non-uniform mask during masked generation. The canvas supplies global structure early in sampling, enabling faster and more coherent frame synthesis. To further stabilize autoregressive sampling, we propose an easy-to-hard curriculum via a motion-aware sampling order that synthesizes relatively stationary regions before attending to highly dynamic ones. We also integrate compositional classifier-free guidance that jointly strengthens the canvas and temporal conditioning to improve generation fidelity. Experiments on the BAIR, UCF-101, and Kinetics-600 benchmarks demonstrate that CanvasMAR produces higher-quality videos with fewer autoregressive steps. On the challenging Kinetics-600 dataset, CanvasMAR achieves remarkable performance among autoregressive models and rivals advanced diffusion-based methods.

Keywords: Video prediction · Masked autoregressive models · Canvas

1 Introduction

Masked generative models have achieved remarkable success in both image generation [5, 31, 32] and video generation [7, 67, 74]. By representing images as tokens and generating them set by set in a random order,⁴ these models achieve

* Corresponding Author.

⁴ For models such as MaskGiT [5], the generation order is not strictly random because it also relies on token probabilities interpreted as confidence scores. However, we adopt a generalized notion of “random” to contrast with strictly predefined orders like raster scan.

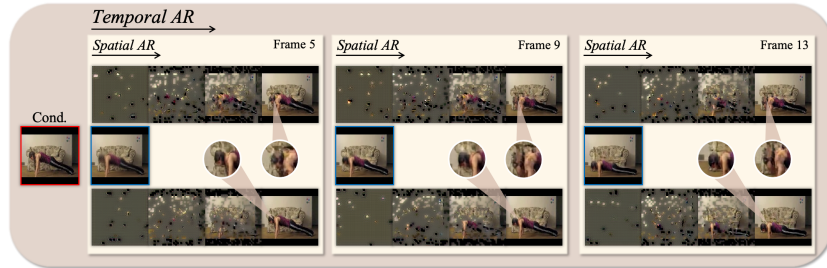


Fig. 1: Video generation with Masked Autoregressive Models using only 8 autoregressive steps per 32×32 latent frame. Frames with red borders (left) denote the conditioning inputs. Without a canvas (top row), the model quickly loses global coherence for the body. Our approach (second and bottom rows) mitigates this by first predicting a blurred canvas (shown in the second row with blue borders) that captures coarse motion and global structure. The canvas then replaces the uniform mask in the masked autoregressive model, allowing global fidelity to be preserved even under an aggressive sampling regime.

higher fidelity and scalability than approaches that rely on predefined orders [13]. Among these approaches, Masked Autoregressive Models (MAR) [13, 32]⁵ pioneer the generation of continuous image tokens with a diffusion head, in contrast to prior works that use discrete tokens [5, 67]. This eliminates the quantization errors inherent in discrete-token masked generative models and avoids the challenges of training high-quality VQ-VAEs [12, 18, 51, 68], demonstrating strong potential both theoretically and empirically.

Extending the MAR paradigm—continuous image tokens with random-order autoregressive generation—to video generation is promising, as evidenced by several recent studies [7, 66, 74]. However, a key challenge remains: MAR follows the MaskGIT [5] sampling paradigm, which begins from a fully masked image and autoregressively generates tokens in a random order. In early stages, when only a few tokens have been generated, the model must generate small sets of tokens at each step to maintain quality. The set size gradually increases only as more tokens are revealed, typically following a cosine schedule [5]. This creates a *trade-off between fidelity and sampling speed*: achieving high-quality generation typically requires significantly many sampling steps, while using only few steps often results in highly distorted outputs—especially for videos, where the temporal dimension further amplifies the issue. As illustrated in Fig. 1, a simple video MAR model exhibits noticeable degradation after only 8 spatial autoregressive steps when generating a 32×32 latent frame (256×256 pixel frame), and the problem worsens as more frames are rolled out.

In this paper, we introduce **CanvasMAR**, a masked autoregressive video prediction model that sustains *high fidelity* while using *few autoregressive steps*

⁵ We adopt the generalized notion of “autoregressive” introduced in [32], which treats masked generation as autoregression along the spatial axis in random order.

per frame. CanvasMAR operates through a two-level autoregressive process: temporally, it generates frames sequentially; spatially, it partitions each frame into image tokens and produces them set by set in an adaptive, motion-aware order. To maintain fidelity with few sampling steps, CanvasMAR first predicts a blurred next frame—the *canvas* (see Fig. 1)—with only one model pass, and replaces the uniform masks in conventional masked generators with these non-uniform *canvas tokens*. The canvas captures the global structure of the target frame, enabling more aggressive yet coherent synthesis. To stabilize sampling, we further introduce an adaptive, motion-aware sampling order for next-frame generation: the model first synthesizes low-motion (near-stationary) regions, then progressively attends to highly dynamic areas, yielding an easy-to-hard curriculum that stabilizes autoregressive sampling and suppresses motion artifacts. We also develop compositional classifier-free guidance [1,9,22] that jointly strengthens the canvas and temporal conditioning, further improving fidelity.

Experiments on standard video prediction datasets—including the lab-scale BAIR [10, 50], the moderate-scale UCF-101 [46], and the large-scale Kinetics-600 [4] benchmarks—validate the effectiveness of our approach. On BAIR and Kinetics-600, CanvasMAR delivers significant gains over prior autoregressive models such as MAGI [74] and rivals strong diffusion-based baselines like DFoT [44], underscoring the potential of global structure-aware masked generative models.

2 Related Work

2.1 Diffusion-Based Video Generative Models

Diffusion models have demonstrated remarkable success in image generation [20, 40, 45], and have since been extended to video generation by treating the temporal axis as an additional dimension alongside the spatial ones [2, 23, 29, 38, 55, 64]. While effective, this paradigm generates entire videos as a whole, which leads to high latency and limited interactivity—two critical drawbacks for applications such as interactive simulators and game environments [3, 14]. To mitigate these issues, recent research has adopted an autoregressive approach, wherein videos are generated sequentially by conditioning on previously generated clean frames. This design enables interactivity and supports the generation of longer, temporally coherent videos [17, 26, 34, 36, 41, 44, 65, 71]. However, these methods still remain diffusion-based, which generate individual frames or chunks as a whole through iterative frame-level denoising. In contrast, token-based autoregressive models that this work focuses on directly learn token-level distributions and produce image tokens, making them more natively compatible with large language models and thus better suited for multimodal model designs [27, 58].

2.2 Autoregressive Video Generation

An alternative line of work decomposes video frames into image tokens, shifting the generative task from producing full frames to predicting sequences of tokens.

Many approaches in this direction adopt quantized tokens, typically following paradigms such as next-token prediction [24, 27, 47, 58, 60, 63] or masked generative modeling [3, 16, 52, 57, 67, 68]. However, as observed by Yu *et al.* [68], these paradigms rely on carefully designed and trained VQ-VAEs [12, 51], which inevitably introduce quantization errors. Inspired by Masked Autoregressive Models (MAR) [13, 32], a growing body of work—representative works including NOVA [7], VideoMAR [66], and MAGI [74]—adapts MAR to video generation, which directly generate continuous image tokens and achieve remarkable generation performance.

2.3 Cascaded Generation

The closest line of work that shares a similar idea with *canvas* is cascaded generation. Cascaded generation frameworks decompose synthesis into stages that progressively increase resolution or temporal span [15, 19, 21, 42, 59, 69, 72]. Early image pipelines such as Cascaded Diffusion [21] train a low-resolution base model to capture global semantics before invoking specialized super-resolution and detail-enhancement modules. Such a coarse-to-fine strategy improves sample quality but requires separate networks, schedulers, and guidance hyperparameters per stage. The same underlying insight also extends to autoregressive approaches like VAR [48] for next-scale prediction and to masked generative models like HiMAR [72], though implementations differ. Recent large-scale video systems includes FlashVideo [69] and Waver [70] also adopt similar ideas for fast and high-fidelity video generation. However, **CanvasMAR is fundamentally different from these cascaded methods**: these works produce *multi-step generated samples* $x \sim p(x)$ for each low-resolution image/frame x , whereas CanvasMAR produces a *one-step predicted expectation* $\mathbb{E}[x]$ for the next frame x , which is computationally much more efficient and tailored for video MAR models.

3 Preliminaries

3.1 Factorizing Video Generation

In this paper, we focus on autoregressive video prediction. A video is denoted as $V \in \mathbb{R}^{N \times H \times W \times 3}$, which consists of N frames $[f^{(1)}, f^{(2)}, \dots, f^{(N)}]$ of height H and width W . We employ latent generation [40]; however, for simplicity, we retain pixel-level notation. Autoregressive video generation models the video distribution via the following *temporal* factorization:

$$p(V) = \prod_{i=1}^N p(f^{(i)} | f^{(<i)}), \quad (1)$$

where $f^{(<i)} = \{f^{(1)}, f^{(2)}, \dots, f^{(i-1)}\}$ denotes all preceding frames. Each frame $f^{(i)}$ is further decomposed into a sequence of image tokens in raster order,

$f^{(i)} = [x_1^{(i)}, x_2^{(i)}, \dots, x_n^{(i)}]$. In standard autoregressive generation [24, 63], tokens are generated in raster order token-by-token:

$$p(f^{(i)} | f^{(<i)}) = \prod_{j=1}^n p(x_j^{(i)} | f^{(<i)}, x_{<j}^{(i)}), \quad (2)$$

where $x_{<j}^{(i)} = \{x_1^{(i)}, x_2^{(i)}, \dots, x_{j-1}^{(i)}\}$ denotes the tokens already generated within frame i .

Masked generative paradigms [5, 7, 32] generate tokens set by set in a random order. Specifically, the n tokens are randomly partitioned into K sets of sizes $[n_1, n_2, \dots, n_K]$, with cumulative index $s_k = \sum_{m=1}^k n_m$ and $s_0 = 0$, $s_K = n$. This factorization introduces *spatial* autoregression:

$$p(f^{(i)} | f^{(<i)}) = \prod_{k=1}^K p(X_k^{(i)} | f^{(<i)}, X_1^{(i)}, X_2^{(i)}, \dots, X_{k-1}^{(i)}), \quad (3)$$

where each token set is defined as $X_k^{(i)} = \{x_{\tau(s_{k-1}+1)}^{(i)}, x_{\tau(s_{k-1}+2)}^{(i)}, \dots, x_{\tau(s_k)}^{(i)}\}$ where $\tau \sim \mathcal{S}_n$ denotes a random permutation sampled from the symmetric group \mathcal{S}_n , i.e., the set of all permutations of the index sequence $[1, 2, \dots, n]$. This sampling introduces stochasticity into the generation process.

3.2 Masked Autoregressive Models with Continuous Tokens

Unlike conventional autoregressive generative models that produce quantized image tokens [24, 63] using categorical distributions, MAR [32] directly generates continuous image tokens using a diffusion head, which models token distributions conditioned on token embeddings. Formally, the distribution in Eq. (3) is further factorized as:

$$p(X_k^{(i)} | f^{(<i)}, X_{<k}^{(i)}) := p(X_k^{(i)} | Z_k^{(i)}) \cdot p(Z_k^{(i)} | f^{(<i)}, X_{<k}^{(i)}), \quad (4)$$

where $Z_k^{(i)} = \{z_{\tau(s_{k-1}+1)}^{(i)}, z_{\tau(s_{k-1}+2)}^{(i)}, \dots, z_{\tau(s_k)}^{(i)}\}$ denotes the token embeddings, and $X_{<k}^{(i)} = \{X_1^{(i)}, X_2^{(i)}, \dots, X_{k-1}^{(i)}\}$. The conditional distribution $p(X_k^{(i)} | Z_k^{(i)}) = \prod_{j=s_{k-1}+1}^{s_k} p(x_j^{(i)} | z_j^{(i)})$ models per-token outputs given the embeddings, where correlations between tokens are captured when computing the embeddings. In practice, $p(Z_k^{(i)} | f^{(<i)}, X_1^{(i)}, X_2^{(i)}, \dots, X_{k-1}^{(i)})$ is parameterized by a Vision Transformer [8] that learns token-wise embeddings as δ distribution, while $p(x_j^{(i)} | z_j^{(i)})$ is modeled by a lightweight MLP-based diffusion head that conditions on $z_j^{(i)}$ to generate $x_j^{(i)}$ [32].

4 Methods

4.1 Factorized Temporal and Spatial Autoregression

We design our model to generate videos through a factorized temporal-spatial autoregressive framework, as illustrated in Fig. 2. For clarity, we denote hidden

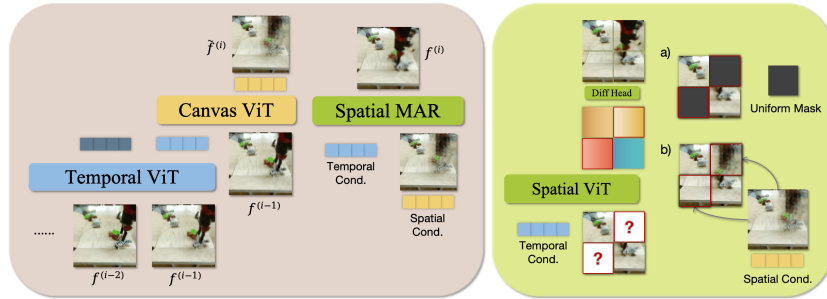


Fig. 2: Left: Inference procedure of CANVASMAR. The framework consists of three modules: *Temporal ViT*, *Canvas ViT*, and *Spatial MAR*. The *Temporal ViT* encodes the historical frames and produces a temporal embedding that serves as a temporal condition for both the *Canvas ViT* and the *Spatial MAR*. The *Canvas ViT* takes the temporal embedding together with the most recent frame to predict a coarse *canvas* in one go, i.e., the initial guess of the future frame, which, along with the temporal embedding, provides spatial conditioning for the *Spatial MAR*. **Right:** Training procedure of the *Spatial MAR*. A *Spatial ViT* learns to reconstruct randomly masked regions within frames. Unlike vanilla *MAR* (a), which uses a single learnable mask embedding for all regions, *CanvasMAR* replaces this with the predicted *canvas* (b), offering a more informative and adaptive conditioning signal.

representations by z and refer to the temporal and canvas latents as z_t and z_c . Specifically, *CanvasMAR* proceeds in two stages for generating the next frame i : 1) a temporal embedding $z_t^{(i)} \in \mathbb{R}^{n \times d}$, where n denotes the number of frame tokens and d the hidden dimension, is autoregressively generated for frame i , using a *Temporal ViT* [8] that conditions on all past frames $f^{(<i)}$; 2) this temporal embedding is provided as a conditioning sequence to the *Spatial MAR*, implemented as a masked autoregressive model [32], which generates image tokens set by set for the next frame $f^{(i)}$.

The attention mask of the *Temporal ViT* follows the *hybrid* structure of Deng *et al.* [7], Yu *et al.* [66]—causal across frames and bidirectional within each frame. This design preserves temporal causality while maintaining comprehensive spatial perception within frames, and it enables frame-level *KV caching*, further accelerating generation.

We note that this temporal-spatial factorization *preserves both training and inference efficiency*, unlike models that process temporal and spatial sequences uniformly [66, 74]: 1) During training, tokens within each frame can be independently masked, and all masked frames contribute to the loss in parallel, analogous to decoder-only language models [49, 68]. In contrast, models without factorized autoregression can mask tokens only in the last frame of a sequence and compute loss of the only masked frame [66], leading to inefficient training. A potential remedy, as explored in *MAGI* [74], is to duplicate “clean” frames for each frame in the sequence and design a corresponding attention mask, which doubles the sequence length and substantially increases memory usage. 2) Dur-

ing inference, the temporal embedding z_t captures motion information necessary to guide next-frame generation. As a result, spatial token generation needs only attend to this fixed-length temporal embedding rather than all previously generated image tokens, whose size grows with sequence length.

4.2 Bridging Fast Temporal Autoregression and Slow Spatial Autoregression with Canvas

As shown in Fig. 1, the absence of an initial global estimate of the target frame severely limits the size of the early token sets, i.e., s_i in Eq. (3) has to be small for small i . In video generation, this further degrades both quality and speed. To address it, we introduce the *canvas* between temporal autoregression and spatial autoregression, as illustrated in Fig. 2.

Specifically, after obtaining the temporal embedding $z_t^{(i)}$, we first pass it through the *Canvas ViT* module instead of feeding it directly to the Spatial MAR. This module predicts a blurred, coarse version of the next frame $z_c^{(i)}$, which serves as an explicit *spatial condition* for subsequent modules. The Spatial MAR then receives both the temporal condition $z_t^{(i)}$ and the spatial canvas embedding $z_c^{(i)}$ to predict the next frame, as shown on the right side of Fig. 2.

Concretely, the Canvas ViT takes the temporal representation $z_t^{(i)}$ together with the most recent frame $f^{(i-1)}$ as input and outputs a canvas embedding $z_c^{(i)} \in \mathbb{R}^{n \times d}$, representing an initial guess of the next frame $f^{(i)}$. To supervise this process, we introduce a canvas reconstruction loss:

$$\mathcal{L}_{\text{canvas}} = \mathbb{E}_{f^{(i+1)}} \left[\sum_{j=1}^n \|f_{\theta}^{\text{canvas}}(z_{c,j}^{(i)}) - x_j^{(i)}\|_2^2 \right], \quad (5)$$

where $z_{c,j}^{(i)}$ denotes the j -th row of $z_c^{(i)}$, and $f_{\theta}^{\text{canvas}}$ is a simple linear projection layer that supervises each patch embedding $z_c^{(i)}$ to match the corresponding j -th patch in the ground-truth future frame $x_j^{(i)}$.

We note that, unlike the Spatial MAR—which is inherently slower and stochastic—the Canvas ViT is *fast and deterministic*: given the same temporal embedding $z_t^{(i)}$ and previous frame $f^{(i-1)}$, it always produces the same canvas. Theoretically, **the optimal Canvas ViT approximates the expected future frame** $\mathbb{E}_{f^{(i)} \sim p(f^{(i)} | f^{(<i)})} [f^{(i)}]$ given past frames, effectively producing a superposition of plausible outcomes. This initialization allows the Spatial MAR to maintain global coherence early on and quickly “collapse” onto one plausible future frame.

4.3 Motion-Aware Adaptive Sampling Order

The canvas approximates the conditional expectation of the next frame given the history. Consequently, highly dynamic regions can appear blurrier than stationary ones because they exhibit more uncertainty. Generating multiple patches

in such blur regions simultaneously during early sampling steps can therefore be suboptimal, even with the canvas condition. We therefore design a motion-aware adaptive sampling order that prioritizes low-motion areas early and gradually attends to high-motion areas, implementing an easy-to-hard curriculum that stabilizes sampling and reduces motion artifacts.

Specifically, we add a lightweight *staticness head* $f_{\theta}^{\text{static}}$ to the Canvas ViT that predicts a nonnegative scalar score per canvas patch, where larger values indicate lower motion. The score is supervised with a training-time loss that resembles confidence prediction in AlphaFold [28]. Formally, let the per-patch canvas reconstruction error

$$\ell_j^{(i)} = \|f_{\theta}^{\text{canvas}}(z_{c,j}^{(i)}) - x_j^{(i)}\|_2^2. \quad (6)$$

We define the target staticness as $s_j^{(i)} = \exp(-\ell_j^{(i)})$, where $0 \leq s_j^{(i)} \leq 1$. We then train with an MSE loss

$$\mathcal{L}_{\text{static}} = \mathbb{E}_{f^{(i+1)}} \left[\sum_{j=1}^n (f_{\theta}^{\text{static}}(z_{c,j}^{(i)}) - \text{stop}(s_j^{(i)}))^2 \right], \quad (7)$$

where $f_{\theta}^{\text{static}}$ denotes a simple motion head (a linear layer followed by a sigmoid) that probes each patch embedding to predict staticness, and $\text{stop}(\cdot)$ indicates stop-gradient operation. Intuitively, with f^{canvas} predicting the expectation of a future patch, f^{static} estimates a quantity related to the variance of the corresponding patch.

In MAR [32], sampling proceeds in a purely random order. Although this aligns with the training distribution of masked generative modeling [32], it is suboptimal for next-frame generation because of the function-reuse approximation error (i.e., reusing a function evaluation for both regions with high and low motion) [73]. We therefore treat the staticness scores as confidence values that bias the sampling order toward low-motion regions in early steps and gradually revert to random order in later steps. We follow the temperature-annealing method of MaskGiT [5] to retain stochasticity.

4.4 Compositional Classifier-Free Guidance

Guidance is known to significantly improve generation fidelity [1, 9, 22, 40, 44]. In CanvasMAR, the introduction of the canvas provides a significant spatial condition in addition to the temporal one. We therefore adopt compositional classifier-free guidance to enhance robustness under this expanded conditioning setup.

For the Spatial MAR, the generative distribution is $p(f^{(i)} | z_c^{(i)}, z_t^{(i)})$, where $z_c^{(i)}$ denotes the canvas condition and $z_t^{(i)}$ denotes the temporal condition. We decompose the distribution as

$$p(f^{(i)} | z_c^{(i)}, z_t^{(i)}) \propto p(f^{(i)}) p(z_t^{(i)} | f^{(i)}) p(z_c^{(i)} | f^{(i)}, z_t^{(i)}),$$

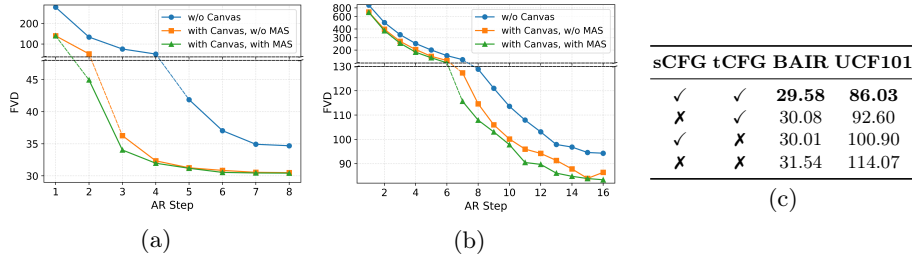


Fig. 3: Component-level analysis. In the first two figures, classifier-free guidance is not used, and MAS represents the motion-aware sampling order. (a) Effectiveness of canvas and motion-aware sampling on BAIR. (b) Effectiveness of canvas and motion-aware sampling on UCF-101. (c) Effectiveness of compositional classifier-free guidance, where sCFG represents spatial (canvas) CFG, and tCFG represents the temporal CFG. The metric is FVD; the lower, the better.

and apply compositional CFG [1, 9] to up-weight both the spatial and temporal posteriors:

$$p^{(w_s, w_t)}(f^{(i)} | z_c^{(i)}, z_t^{(i)}) := p(f^{(i)}) p(z_t^{(i)} | f^{(i)})^{w_t} p(z_c^{(i)} | f^{(i)}, z_t^{(i)})^{w_s}, \quad (8)$$

where w_s and w_t denote the guidance scales for the spatial and temporal conditions, respectively. Intuitively, w_s and w_t increase the likelihood that the generated frame $f^{(i)}$ conforms to the spatial prior $z_c^{(i)}$ and the temporal-consistency constraint $z_t^{(i)}$. Eq. (8) leads to the following score combination:

$$\begin{aligned} \mathbf{s}^{(w_s, w_t)} &= \nabla_{f^{(i)}} \log p^{(w_s, w_t)}(f^{(i)} | z_c^{(i)}, z_t^{(i)}) \\ &= \mathbf{s}_\emptyset + w_t (\mathbf{s}_t - \mathbf{s}_\emptyset) + w_s (\mathbf{s}_{t,s} - \mathbf{s}_t), \end{aligned} \quad (9)$$

where $\mathbf{s}_\emptyset = \nabla \log p(f^{(i)})$ is the unconditional score, $\mathbf{s}_t = \nabla \log p(f^{(i)} | z_t^{(i)})$ is the temporal-only score, and $\mathbf{s}_{t,s} = \nabla \log p(f^{(i)} | z_t^{(i)}, z_c^{(i)})$ is the fully conditioned score.

We obtain $\{\mathbf{s}_\emptyset, \mathbf{s}_t, \mathbf{s}_{t,s}\}$ via three forward passes of the Spatial MAR head that differ only in their conditioning inputs (unconditional, temporal-only, and temporal+spatial). We then combine the predicted scores according to Eq. (9) before updating tokens.

To enable CFG at inference, we adopt classifier-free training by randomly dropping conditions: with 5% probability we replace the spatial condition with a uniform mask [5]; with 5% probability we replace the temporal sequence with a learnable temporal vector; with 5% probability we drop both; otherwise we keep both.

5 Experiments

5.1 Settings

Model Implementation. We implement CanvasMAR on the NOVA [7] codebase with three additional changes: (1) a flow head trained with flow matching [33, 35] instead of DDPM [20]; (2) expert LayerNorm [64] that treats the conditioning sequence, clean tokens, and mask tokens separately, or MM-DiT [11] that treats the clean and mask tokens separately; and (3) removal of the Scale-and-Shift layer for the temporal embedding [7].

Training Objective. According to Sec. 4, training CanvasMAR involves three objectives: (1) the canvas-masked reconstruction objective for the Spatial MAR head \mathcal{L}_{MAR} ; (2) the canvas reconstruction loss $\mathcal{L}_{\text{canvas}}$ in Eq. (5); and (3) the staticness prediction loss $\mathcal{L}_{\text{static}}$ in Eq. (7). We therefore optimize a weighted objective:

$$\mathcal{L}_{\text{total}} = \mathcal{L}_{\text{MAR}} + \lambda_c \mathcal{L}_{\text{canvas}} + \lambda_s \mathcal{L}_{\text{static}}, \quad (10)$$

and set both weights λ_c and λ_s to 0.1 in all experiments.

Tasks and Datasets. We evaluate CanvasMAR on video prediction tasks, where one or more context frames are given and the goal is to forecast subsequent frames. Our experiments span three datasets of increasing scale and complexity: 1) **BAIR**. The BAIR dataset [10, 50] is a toy benchmark containing 43K training videos and 256 evaluation videos of a robot arm pushing objects within a static camera view. 2) **UCF-101**. UCF-101 [46] is a moderate-scale real-world dataset with over 13,000 clips across 101 human action classes. 3) **Kinetics-600**. The Kinetics-600 dataset [4] is a large-scale collection of diverse real-world videos spanning 600 human action categories. It contains approximately 400K training clips and serves as a challenging benchmark for large-scale video generation. Since UCF-101 is typically used for conditional generation without context frames [74], which CanvasMAR does not currently support (see clarification in Sec. 6), we report comparisons only against the baseline method we implemented. For BAIR and Kinetics-600, we provide system-level comparisons with prior art. See Appendix A for more details.

5.2 Component-Level Analysis

Effectiveness of the canvas. Since the canvas module is central to CanvasMAR, we first study its impact. To achieve this, we train a model identical to CanvasMAR but without the canvas component *from scratch*, and compare the two under identical experimental settings except for the use of the canvas. Results on the BAIR and UCF-101 datasets (Fig. 3 (a) and (b), blue and orange lines) show that the canvas-equipped model consistently outperforms its non-canvas counterpart across all autoregressive step counts. Notably, larger gains appear at small step counts (e.g., 2-4 on the BAIR dataset and 2-8 on the

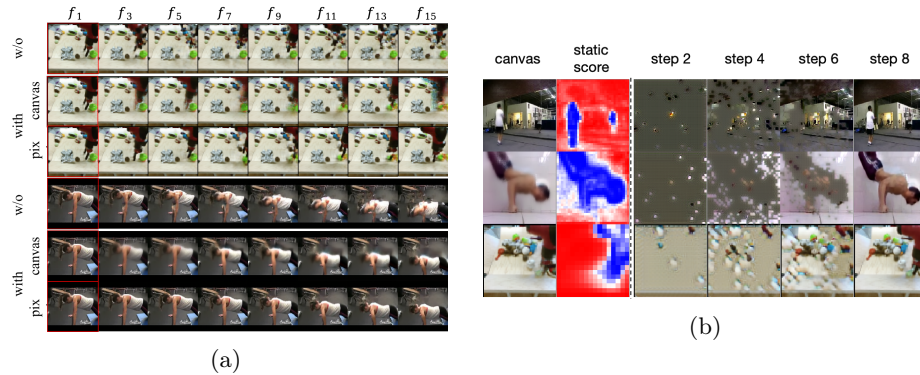


Fig. 4: (a) Qualitative examples of video clips generated by CanvasMAR (bottom two rows in each example) and its non-canvas variant (top row). Upper: 2-step generation on BAIR (16×16 latents); Lower: 8-step generation on UCF-101 (32×32 latents). The canvas-based model better preserves global structure and object coherence. (b) Qualitative illustration of the motion-aware staticness prediction and adaptive sampling schedule. Warmer colors denote regions predicted to remain relatively static and are therefore generated earlier, while cooler colors indicate high-motion regions deferred to later autoregressive steps.

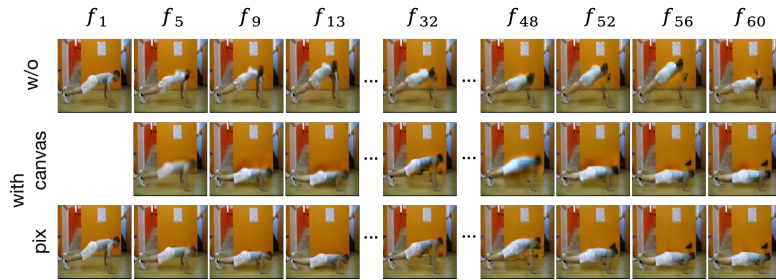


Fig. 5: Qualitative example of longer video generation generated by CanvasMAR and its non-canvas variant.

UCF101 dataset), supporting the importance of a global spatial prior in few-step settings. Qualitative comparisons in Fig. 4 (a) demonstrate that the model without the canvas struggles to maintain global structure and object coherence, whereas the canvas-based model preserves good spatial and temporal consistency in few-step settings. Furthermore, CanvasMAR can generate long videos by autoregressively rolling out frames, and with stable temporal coherence. Fig. 5 presents a 60-frame video (compared to the typical 16-frame evaluation) generated by CanvasMAR and its non-canvas counterpart; here, CanvasMAR again demonstrates consistently better generation.

Effectiveness of adaptive motion-aware sampling. The adaptive motion-aware sampling strategy enables an easy-to-hard curriculum for next-frame gen-

eration. As shown in Fig. 3 (a) and (b) (orange and green lines), it consistently improves performance in fewer-step settings—the case we focus on for efficient sampling. With more sampling steps, each batch of simultaneously generated tokens becomes smaller, reducing conflicts even without adaptive sampling and therefore narrowing the gap as we expected. Qualitative examples in Fig. 4 (b) visualize the predicted staticness map and its induced ordering, showcasing that the lightweight static head successfully captures motion information. After that, low-motion regions (warm colors) are synthesized first, while high-motion regions (cool colors) are deferred to later steps as expected.

Effectiveness of compositional CFG. Fig. 3 (c) summarizes the impact of the spatial and temporal branches of compositional classifier-free guidance. Disabling either branch degrades performance, validating the importance of both guidance for autoregressive video generation.

5.3 System-Level Comparisons

We compare CanvasMAR with well-known diffusion-based and autoregressive video models. Note that each method is categorized by its frame-level generation mechanism—either generating full frames or individual image tokens—which more directly determines visual quality than the temporal generation paradigm (generating an entire video as a whole versus rolling out frames sequentially).

Table 1: System-level comparison on Kinetics-600. FVD↓ at 64×64 (methods with * may be evaluated at 128×128).

Type	Method	FVD↓
GAN	DVD-GAN-FP [6]	69.1
	ThVD-GAN-FP [37]	25.74
Diffusion	VDM [23]	16.2
	RaMViD [25]	16.5
	Rolling Diffusion [41]	5.2
	DFoT* [44]	4.3
Autoregressive	Video Transformer [61]	170
	CogVideo [24]	109.2
	Video VQ-VAE [54]	64.3
	CCVS [30]	55.0
	Phenaki* [52]	36.4
	Transframer [39]	25.4
	MAGVIT [67]	9.9
	MAGVIT-v2 [68]	4.3
	MAGI [74]	11.5
	Ours ($N_{AR} = 10$)	6.3
Ours ($N_{AR} = 11$)	6.3	
Ours ($N_{AR} = 12$)	6.2	

Table 2: System-level comparison on BAIR. FVD↓ at 64×64 . DFVD reports debiased FVD [67].

Type	Method	FVD↓	DFVD↓
GAN	DVD-GAN-FP [6]	109.8	-
	ThVD-GAN-FP [37]	103	-
Diffusion	MCVD [53]	90	-
	RaMViD [25]	84	-
	VDM [23]	66.9	-
AR	Transframer [39]	100	-
	CCVS [30]	99	-
	Phenaki [52]	97	-
	MaskViT [16]	94	-
	NÜWA [62]	87	-
	MAGVIT-L [67]	62	31
	MAGVIT-B [67]	76	48
	Ours ($N_{AR} = 4$)	66.0	26.6
Ours ($N_{AR} = 6$)	65.3	26.5	
Ours ($N_{AR} = 8$)	65.2	26.4	

As shown in Tab. 2, CanvasMAR achieves the second-best FVD on BAIR among autoregressive models, trailing only MAGVIT. However, under the debiased evaluation, CanvasMAR surpasses MAGVIT, achieving *the best performance*. We argue that the debiased setting is much more convincing due to

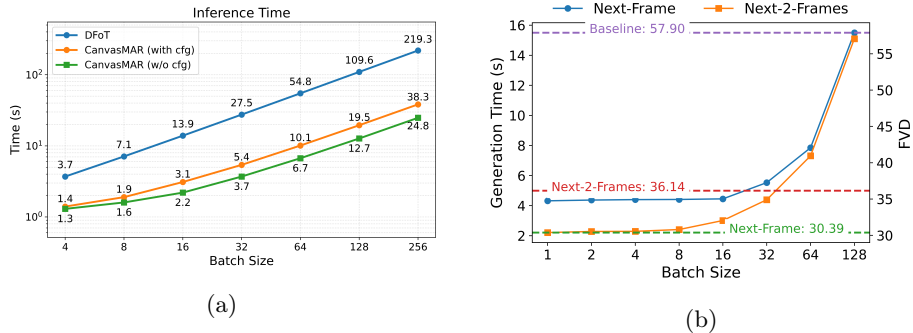


Fig. 6: (a) Inference latency comparison of CanvasMAR and DFoT on K600. CanvasMAR achieves much lower latency than DFoT due to the autoregressive paradigm and fewer-step sampling. (b) Performance and speedup effect of next-group prediction models. No classifier-free guidance is used.

the wider sample distributions, as detailed in Sec. A. Notably, MAGVIT is autoregressive only in the spatial domain, but generates all frames simultaneously without enforcing temporal causality. This design reduces the difficulty of video generation but incurs substantially higher latency. In contrast, CanvasMAR generates frames sequentially—making it more prone to error accumulation—yet it delivers better performance.

On the larger and more challenging Kinetics-600 dataset in Tab. 1, CanvasMAR trails only MAGVIT-v2 [68] among autoregressive models, which likewise does not enforce causality and leverages a more advanced autoencoder. Note that MAGI [74] is a more closely related baseline—both temporally and spatially autoregressive, yet without the canvas mechanism—highlighting the effectiveness of our design.

CanvasMAR also rivals state-of-the-art diffusion models, and with much better efficiency. To illustrate this, we compare inference time with the advanced diffusion model DFoT [44] in Fig. 6 (a). CanvasMAR is about $5.7 \times$ faster at the largest batch size (GPU fully utilized), highlighting the efficiency advantage of few-step autoregressive sampling. Fig. 6 (a) reports latency—the time until the first frame appears—which is often the most relevant metric for interactive applications and one at which autoregressive models typically excel. We further show that even when considering total generation time (see Fig. 8 in Appendix A), CanvasMAR remains about $2.7 \times$ faster than DFoT.

Further increasing the sampling steps of CanvasMAR on both datasets yields only minimal performance gains, indicating that only a few steps are sufficient for CanvasMAR. In contrast, the non-canvas baseline shown in Fig. 3 fails to surpass the CanvasMAR even with more sampling steps.

5.4 Next-Group Frame Prediction

In diffusion-based autoregressive models [26, 34, 44, 65], predicting multiple upcoming frames (e.g., chunks) jointly is common. For token-based autoregressive models, models typically generate frames one at a time [7], where next-group prediction often leads to severe performance degradation. However, with the introduction of the canvas, we find next-group frame prediction to be stable, enabling faster generation with limited quality loss.

Empirically, we fine-tune a next-group frame prediction model (with a group size of 2) from a well-trained next-frame prediction model on BAIR, requiring only about 10% of the original training cost to converge. This indicates that substantial knowledge is transferred between next-frame and next-group settings. See Appendix B for more details of the model architecture.

As shown in Fig. 6 (b), the next-2-frame model exhibits substantial speedups at smaller batch sizes compared to the next-frame model and converges to similar throughput at higher batch sizes. When the batch size becomes large, both models fully utilize the available GPU resources and, thanks to KV caching, reach comparable parallel efficiency. In practical scenarios, however, users typically generate only a few videos and expect low latency, where the next-2-frame prediction model is particularly advantageous. Furthermore, we train a next-2-frame prediction model without the canvas (purple curve), and our canvas-based model performs significantly better when transferred to next-group prediction because the canvas provides strong structural priors for multiple future frames.

6 Conclusion and Limitations

Conclusions. We presented CanvasMAR, a masked autoregressive video prediction framework that improves both quality and efficiency through a canvas-based conditioning mechanism. By generating a blurred global estimate of the next frame before spatial token generation, CanvasMAR bridges the gap between fast temporal and slow spatial autoregression, reducing the generation step in conventional MAR models and improving fidelity. Experiments on BAIR and Kinetics-600 confirm that CanvasMAR achieves competitive or superior FVD scores with fewer autoregressive steps, outperforming most prior autoregressive baselines.

Limitations. Despite its strong performance, CanvasMAR has several limitations. First, CanvasMAR is primarily evaluated on video prediction tasks, which assume the availability of previous frames. This focus stems from the core contribution of the paper—the canvas mechanism—which relies on preceding frames. However, this is not an inherent limitation of CanvasMAR: it can also generate videos from scratch, as the first frame can always be generated without the canvas mechanism (similar to NOVA [32]). We did not evaluate this scenario as it lies outside the main contribution of our work. Second, when predicting videos with substantial motion, CanvasMAR can produce severely distorted results, as

shown in Fig. 7 in Appendix Sec. A. One reason is that the initial canvas can be overly blurred for such sequences, which misleads the Spatial MAR and leaves it unable to fully correct these artifacts. Scaling up the model may improve its self-correction ability, especially considering that our largest Spatial MAR has only half the layers of NOVA [7]. Future work will also explore scaling CanvasMAR to text-conditioned and multimodal settings.

References

1. Brooks, T., Holynski, A., Efros, A.A.: Instructpix2pix: Learning to follow image editing instructions. In: Proceedings of the IEEE/CVF conference on computer vision and pattern recognition. pp. 18392–18402 (2023)
2. Brooks, T., Peebles, B., Holmes, C., DePue, W., Guo, Y., Jing, L., Schnurr, D., Taylor, J., Luhman, T., Luhman, E., et al.: Video generation models as world simulators. *OpenAI Blog* **1**(8), 1 (2024)
3. Bruce, J., Dennis, M.D., Edwards, A., Parker-Holder, J., Shi, Y., Hughes, E., Lai, M., Mavalankar, A., Steigerwald, R., Apps, C., et al.: Genie: Generative interactive environments. In: Forty-first International Conference on Machine Learning (2024)
4. Carreira, J., Noland, E., Banki-Horvath, A., Hillier, C., Zisserman, A.: A short note about kinetics-600. *arXiv preprint arXiv:1808.01340* (2018)
5. Chang, H., Zhang, H., Jiang, L., Liu, C., Freeman, W.T.: Maskgit: Masked generative image transformer. In: Proceedings of the IEEE/CVF conference on computer vision and pattern recognition. pp. 11315–11325 (2022)
6. Clark, A., Donahue, J., Simonyan, K.: Adversarial video generation on complex datasets. *arXiv preprint arXiv:1907.06571* (2019)
7. Deng, H., Pan, T., Diao, H., Luo, Z., Cui, Y., Lu, H., Shan, S., Qi, Y., Wang, X.: Autoregressive video generation without vector quantization. *arXiv preprint arXiv:2412.14169* (2024)
8. Dosovitskiy, A., Beyer, L., Kolesnikov, A., Weissenborn, D., Zhai, X., Unterthiner, T., Dehghani, M., Minderer, M., Heigold, G., Gelly, S., et al.: An image is worth 16x16 words: Transformers for image recognition at scale. *arXiv preprint arXiv:2010.11929* (2020)
9. Du, Y., Kaelbling, L.: Compositional generative modeling: A single model is not all you need. *arXiv preprint arXiv:2402.01103* (2024)
10. Ebert, F., Finn, C., Lee, A.X., Levine, S.: Self-supervised visual planning with temporal skip connections. *CoRL* **12**(16), 23 (2017)
11. Esser, P., Kulal, S., Blattmann, A., Entezari, R., Müller, J., Saini, H., Levi, Y., Lorenz, D., Sauer, A., Boesel, F., et al.: Scaling rectified flow transformers for high-resolution image synthesis. In: Forty-first international conference on machine learning (2024)
12. Esser, P., Rombach, R., Ommer, B.: Taming transformers for high-resolution image synthesis. In: Proceedings of the IEEE/CVF conference on computer vision and pattern recognition. pp. 12873–12883 (2021)
13. Fan, L., Li, T., Qin, S., Li, Y., Sun, C., Rubinstein, M., Sun, D., He, K., Tian, Y.: Fluid: Scaling autoregressive text-to-image generative models with continuous tokens. *ArXiv abs/2410.13863* (2024)
14. Feng, R., Zhang, H., Yang, Z., Xiao, J., Shu, Z., Liu, Z., Zheng, A., Huang, Y., Liu, Y., Zhang, H.: The matrix: Infinite-horizon world generation with real-time moving control. *arXiv preprint arXiv:2412.03568* (2024)

15. Gu, J., Zhai, S., Zhang, Y., Susskind, J.M., Jaitly, N.: Matryoshka diffusion models. In: The Twelfth International Conference on Learning Representations (2023)
16. Gupta, A., Tian, S., Zhang, Y., Wu, J., Martín-Martín, R., Fei-Fei, L.: Maskvit: Masked visual pre-training for video prediction. arXiv preprint arXiv:2206.11894 (2022)
17. Gupta, A., Yu, L., Sohn, K., Gu, X., Hahn, M., Li, F.F., Essa, I., Jiang, L., Lezama, J.: Photorealistic video generation with diffusion models. In: European Conference on Computer Vision. pp. 393–411. Springer (2024)
18. Han, J., Liu, J., Jiang, Y., Yan, B., Zhang, Y., Yuan, Z., Peng, B., Liu, X.: Infinity: Scaling bitwise autoregressive modeling for high-resolution image synthesis. In: Proceedings of the Computer Vision and Pattern Recognition Conference. pp. 15733–15744 (2025)
19. He, J., Xue, T., Liu, D., Lin, X., Gao, P., Lin, D., Qiao, Y., Ouyang, W., Liu, Z.: Venhancer: Generative space-time enhancement for video generation. arXiv preprint arXiv:2407.07667 (2024)
20. Ho, J., Jain, A., Abbeel, P.: Denoising diffusion probabilistic models. *Advances in neural information processing systems* **33**, 6840–6851 (2020)
21. Ho, J., Saharia, C., Chan, W., Fleet, D.J., Norouzi, M., Salimans, T.: Cascaded diffusion models for high fidelity image generation. *Journal of Machine Learning Research* **23**(47), 1–33 (2022)
22. Ho, J., Salimans, T.: Classifier-free diffusion guidance. arXiv preprint arXiv:2207.12598 (2022)
23. Ho, J., Salimans, T., Gritsenko, A., Chan, W., Norouzi, M., Fleet, D.J.: Video diffusion models. *Advances in neural information processing systems* **35**, 8633–8646 (2022)
24. Hong, W., Ding, M., Zheng, W., Liu, X., Tang, J.: Cogvideo: Large-scale pretraining for text-to-video generation via transformers. arXiv preprint arXiv:2205.15868 (2022)
25. Höpfe, T., Mehrjou, A., Bauer, S., Nielsen, D., Dittadi, A.: Diffusion models for video prediction and infilling. arXiv preprint arXiv:2206.07696 (2022)
26. Huang, X., Li, Z., He, G., Zhou, M., Shechtman, E.: Self forcing: Bridging the train-test gap in autoregressive video diffusion. arXiv preprint arXiv:2506.08009 (2025)
27. Jin, Y., Sun, Z., Xu, K., Chen, L., Jiang, H., Huang, Q., Song, C., Liu, Y., Zhang, D., Song, Y., et al.: Video-lavit: Unified video-language pre-training with decoupled visual-motional tokenization. arXiv preprint arXiv:2402.03161 (2024)
28. Jumper, J., Evans, R., Pritzel, A., Green, T., Figurnov, M., Ronneberger, O., Tunyasuvunakool, K., Bates, R., Žídek, A., Potapenko, A., et al.: Highly accurate protein structure prediction with alphafold. *nature* **596**(7873), 583–589 (2021)
29. Kong, W., Tian, Q., Zhang, Z., Min, R., Dai, Z., Zhou, J., Xiong, J., Li, X., Wu, B., Zhang, J., et al.: Hunyuanvideo: A systematic framework for large video generative models. arXiv preprint arXiv:2412.03603 (2024)
30. Le Moing, G., Ponce, J., Schmid, C.: Ccvs: Context-aware controllable video synthesis. *Advances in Neural Information Processing Systems* **34**, 14042–14055 (2021)
31. Li, T., Chang, H., Mishra, S., Zhang, H., Katabi, D., Krishnan, D.: Mage: Masked generative encoder to unify representation learning and image synthesis. In: Proceedings of the IEEE/CVF Conference on Computer Vision and Pattern Recognition. pp. 2142–2152 (2023)
32. Li, T., Tian, Y., Li, H., Deng, M., He, K.: Autoregressive image generation without vector quantization. *Advances in Neural Information Processing Systems* **37**, 56424–56445 (2024)

33. Lipman, Y., Chen, R.T., Ben-Hamu, H., Nickel, M., Le, M.: Flow matching for generative modeling. arXiv preprint arXiv:2210.02747 (2022)
34. Liu, K., Hu, W., Xu, J., Shan, Y., Lu, S.: Rolling forcing: Autoregressive long video diffusion in real time. arXiv preprint arXiv:2509.25161 (2025)
35. Liu, X., Gong, C., Liu, Q.: Flow straight and fast: Learning to generate and transfer data with rectified flow. arXiv preprint arXiv:2209.03003 (2022)
36. Liu, Z., Deng, X., Chen, S., Wang, A., Guo, Q., Han, M., Xue, Z., Chen, M., Luo, P., Yang, L.: Worldweaver: Generating long-horizon video worlds via rich perception. arXiv preprint arXiv:2508.15720 (2025)
37. Luc, P., Clark, A., Dieleman, S., Casas, D.d.L., Doron, Y., Cassirer, A., Simonyan, K.: Transformation-based adversarial video prediction on large-scale data. arXiv preprint arXiv:2003.04035 (2020)
38. Ma, X., Wang, Y., Jia, G., Chen, X., Liu, Z., Li, Y.F., Chen, C., Qiao, Y.: Latte: Latent diffusion transformer for video generation. arXiv preprint arXiv:2401.03048 (2024)
39. Nash, C., Carreira, J., Walker, J., Barr, I., Jaegle, A., Malinowski, M., Battaglia, P.: Transframer: Arbitrary frame prediction with generative models. arXiv preprint arXiv:2203.09494 (2022)
40. Rombach, R., Blattmann, A., Lorenz, D., Esser, P., Ommer, B.: High-resolution image synthesis with latent diffusion models. In: Proceedings of the IEEE/CVF conference on computer vision and pattern recognition. pp. 10684–10695 (2022)
41. Ruhe, D., Heek, J., Salimans, T., Hooeboom, E.: Rolling diffusion models (2024), <https://arxiv.org/abs/2402.09470>
42. Saharia, C., Ho, J., Chan, W., Salimans, T., Fleet, D.J., Norouzi, M.: Image super-resolution via iterative refinement. IEEE transactions on pattern analysis and machine intelligence **45**(4), 4713–4726 (2022)
43. Skorokhodov, I., Tulyakov, S., Elhoseiny, M.: Stylegan-v: A continuous video generator with the price, image quality and perks of stylegan2. In: Proceedings of the IEEE/CVF conference on computer vision and pattern recognition. pp. 3626–3636 (2022)
44. Song, K., Chen, B., Simchowitz, M., Du, Y., Tedrake, R., Sitzmann, V.: History-guided video diffusion. arXiv preprint arXiv:2502.06764 (2025)
45. Song, Y., Sohl-Dickstein, J., Kingma, D.P., Kumar, A., Ermon, S., Poole, B.: Score-based generative modeling through stochastic differential equations. arXiv preprint arXiv:2011.13456 (2020)
46. Soomro, K., Zamir, A.R., Shah, M.: Ucf101: A dataset of 101 human actions classes from videos in the wild. arXiv preprint arXiv:1212.0402 (2012)
47. Sun, P., Jiang, Y., Chen, S., Zhang, S., Peng, B., Luo, P., Yuan, Z.: Autoregressive model beats diffusion: Llama for scalable image generation. arXiv preprint arXiv:2406.06525 (2024)
48. Tian, K., Jiang, Y., Yuan, Z., Peng, B., Wang, L.: Visual autoregressive modeling: Scalable image generation via next-scale prediction. Advances in neural information processing systems **37**, 84839–84865 (2024)
49. Touvron, H., Lavril, T., Izacard, G., Martinet, X., Lachaux, M.A., Lacroix, T., Rozière, B., Goyal, N., Hambro, E., Azhar, F., et al.: Llama: Open and efficient foundation language models. arXiv preprint arXiv:2302.13971 (2023)
50. Unterthiner, T., Van Steenkiste, S., Kurach, K., Marinier, R., Michalski, M., Gelly, S.: Towards accurate generative models of video: A new metric & challenges. arXiv preprint arXiv:1812.01717 (2018)
51. Van Den Oord, A., Vinyals, O., et al.: Neural discrete representation learning. Advances in neural information processing systems **30** (2017)

52. Villegas, R., Babaeizadeh, M., Kindermans, P.J., Moraldo, H., Zhang, H., Saffar, M.T., Castro, S., Kunze, J., Erhan, D.: Phenaki: Variable length video generation from open domain textual description. arXiv preprint arXiv:2210.02399 (2022)
53. Voleti, V., Jolicoeur-Martineau, A., Pal, C.: Mcvcd-masked conditional video diffusion for prediction, generation, and interpolation. *Advances in neural information processing systems* **35**, 23371–23385 (2022)
54. Walker, J., Razavi, A., Oord, A.v.d.: Predicting video with vqvae. arXiv preprint arXiv:2103.01950 (2021)
55. Wan, T., Wang, A., Ai, B., Wen, B., Mao, C., Xie, C.W., Chen, D., Yu, F., Zhao, H., Yang, J., et al.: Wan: Open and advanced large-scale video generative models. arXiv preprint arXiv:2503.20314 (2025)
56. Wang, J., Jiang, Y., Yuan, Z., Peng, B., Wu, Z., Jiang, Y.G.: Omnitokenizer: A joint image-video tokenizer for visual generation. *Advances in Neural Information Processing Systems* **37**, 28281–28295 (2024)
57. Wang, X., Zhu, Z., Huang, G., Wang, B., Chen, X., Lu, J.: Worlddreamer: Towards general world models for video generation via predicting masked tokens. arXiv preprint arXiv:2401.09985 (2024)
58. Wang, X., Zhang, X., Luo, Z., Sun, Q., Cui, Y., Wang, J., Zhang, F., Wang, Y., Li, Z., Yu, Q., et al.: Emu3: Next-token prediction is all you need. arXiv preprint arXiv:2409.18869 (2024)
59. Wang, Y., Chen, X., Ma, X., Zhou, S., Huang, Z., Wang, Y., Yang, C., He, Y., Yu, J., Yang, P., et al.: Lavie: High-quality video generation with cascaded latent diffusion models. *International Journal of Computer Vision* **133**(5), 3059–3078 (2025)
60. Wang, Y., Xiong, T., Zhou, D., Lin, Z., Zhao, Y., Kang, B., Feng, J., Liu, X.: Loong: Generating minute-level long videos with autoregressive language models. arXiv preprint arXiv:2410.02757 (2024)
61. Weissenborn, D., Täckström, O., Uszkoreit, J.: Scaling autoregressive video models. arXiv preprint arXiv:1906.02634 (2019)
62. Wu, C., Liang, J., Ji, L., Yang, F., Fang, Y., Jiang, D., Duan, N.: Nüwa: Visual synthesis pre-training for neural visual world creation. In: *European conference on computer vision*. pp. 720–736. Springer (2022)
63. Yan, W., Zhang, Y., Abbeel, P., Srinivas, A.: Videogpt: Video generation using vq-vae and transformers. arXiv preprint arXiv:2104.10157 (2021)
64. Yang, Z., Teng, J., Zheng, W., Ding, M., Huang, S., Xu, J., Yang, Y., Hong, W., Zhang, X., Feng, G., et al.: Cogvideox: Text-to-video diffusion models with an expert transformer. arXiv preprint arXiv:2408.06072 (2024)
65. Yin, T., Zhang, Q., Zhang, R., Freeman, W.T., Durand, F., Shechtman, E., Huang, X.: From slow bidirectional to fast autoregressive video diffusion models. In: *Proceedings of the Computer Vision and Pattern Recognition Conference*. pp. 22963–22974 (2025)
66. Yu, H., Gong, B., Yuan, H., Zheng, D., Chai, W., Chen, J., Zheng, K., Zhao, F.: Videomar: Autoregressive video generatio with continuous tokens. arXiv preprint arXiv:2506.14168 (2025)
67. Yu, L., Cheng, Y., Sohn, K., Lezama, J., Zhang, H., Chang, H., Hauptmann, A.G., Yang, M.H., Hao, Y., Essa, I., et al.: Magvit: Masked generative video transformer. In: *Proceedings of the IEEE/CVF Conference on Computer Vision and Pattern Recognition*. pp. 10459–10469 (2023)
68. Yu, L., Lezama, J., Gundavarapu, N.B., Versari, L., Sohn, K., Minnen, D., Cheng, Y., Birodkar, V., Gupta, A., Gu, X., et al.: Language model beats diffusion-tokenizer is key to visual generation. arXiv preprint arXiv:2310.05737 (2023)

69. Zhang, S., Li, W., Chen, S., Ge, C., Sun, P., Zhang, Y., Jiang, Y., Yuan, Z., Peng, B., Luo, P.: Flashvideo: Flowing fidelity to detail for efficient high-resolution video generation. arXiv preprint arXiv:2502.05179 (2025)
70. Zhang, Y., Yang, H., Zhang, Y., Hu, Y., Zhu, F., Lin, C., Mei, X., Jiang, Y., Peng, B., Yuan, Z.: Waver: Wave your way to lifelike video generation. arXiv preprint arXiv:2508.15761 (2025)
71. Zhang, Y., Jiang, J., Ma, G., Lu, Z., Huang, H., Yuan, J., Duan, N.: Generative pre-trained autoregressive diffusion transformer. arXiv preprint arXiv:2505.07344 (2025)
72. Zheng, G., Li, Y., Pan, Y., Deng, J., Yao, T., Zhang, Y., Mei, T.: Hierarchical masked autoregressive models with low-resolution token pivots. arXiv preprint arXiv:2505.20288 (2025)
73. Zheng, K., Chen, Y., Mao, H., Liu, M.Y., Zhu, J., Zhang, Q.: Masked diffusion models are secretly time-agnostic masked models and exploit inaccurate categorical sampling. arXiv preprint arXiv:2409.02908 (2024)
74. Zhou, D., Sun, Q., Peng, Y., Yan, K., Dong, R., Wang, D., Ge, Z., Duan, N., Zhang, X.: Taming teacher forcing for masked autoregressive video generation. In: Proceedings of the Computer Vision and Pattern Recognition Conference. pp. 7374–7384 (2025)

A Experiment Details

Training and Model Details. All models are trained on NVIDIA A100 GPUs. Comprehensive model configurations and hyperparameters are listed in Tab. 3.

Sampling Protocols As noted by Skorokhodov *et al.* [43], the sampling procedure can significantly influence FVD scores. To ensure fair comparisons, we follow the sampling strategies used in prior work:

- **BAIR:** For each of the 256 test videos, we use the first frame as the conditioning input and the subsequent 16-frame segment as the real distribution. We then draw K synthetic 16-frame clips per conditioning frame, resulting in $256 \times K$ generated clips in the fake distribution. Following Yu *et al.* [67], we also report the *debiased FVD* by randomly sampling one conditioning frame per test video and redefining the real distribution accordingly. Repeating this procedure 100 times per video again yields $256 \times K$ generated clips. Unless otherwise specified, we set $K = 20$ and report only the debiased FVD. For system-level comparisons, we align with prior work by using $K = 100$ and reporting both standard and debiased FVD scores.
- **UCF-101:** We randomly sample 5K test videos and, for each, select a random 16-frame clip to define the real distribution, using the preceding 1 frame as a condition to generate one 16-frame clip for the fake distribution.
- **Kinetics-600:** We randomly sample K test videos and, for each, select a random 16-frame clip to define the real distribution, using the preceding 5 frames as conditions to generate one 16-frame clip for the fake distribution. For the system-level study, $K = 50000$, which aligns with previous works. For ablation studies, we set $K = 10000$.

Inference Time For completeness, we report the full generation time comparison in Fig. 8.

Failure Case of CanvasMAR CanvasMAR show sub-optimal performance on highly dynamic video predictions. See Fig. 7.

Canvas Augmentation The canvas is predicted in a single pass, unlike iterative generative models that refine outputs across multiple steps. This design introduces two primary sources of error. First, inaccuracies in the previously generated frame can mislead the Canvas ViT, compounding errors in the next canvas prediction. Second, even with an accurate previous frame, the one-pass Canvas ViT may produce overly blurred or imprecise canvases, which can confuse the Spatial MAR and amplify artifacts.

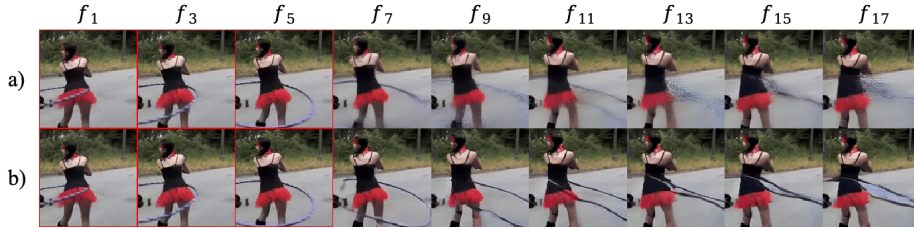


Fig. 7: Failure case of CanvasMAR for videos exhibiting substantial motion. a) The predicted canvas. b) The generated frame.

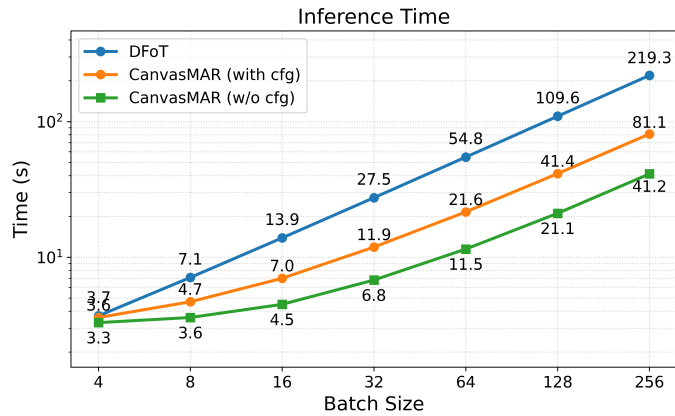


Fig. 8: Inference time comparison of CanvasMAR and DFoT on Kinetics-600. CanvasMAR achieves much lower generation time than DFoT due to the fewer-step sampling.

To mitigate these effects, we additionally adopt a noise-based augmentation strategy inspired by cascaded generation [21, 69]. When feeding the most recent frame $f^{(i-1)}$ into the Canvas ViT, we add Gaussian noise:

$$f_{\text{aug}}^{(i-1)} = f^{(i-1)} \cdot (1 - r) + \epsilon \cdot r, \quad (11)$$

where ϵ denotes Gaussian noise and r is an interpolation coefficient. Similarly, we perturb the canvas embedding:

$$z_{c,\text{aug}}^{(i)} = z_c^{(i)} \cdot (1 - r') + \epsilon' \cdot r', \quad (12)$$

where ϵ' and r' denote another Gaussian noise term and interpolation coefficient. These augmentations simulate instability in previously generated frames and canvases, encouraging both the Canvas ViT and the Spatial MAR to remain robust under imperfect conditions. During training, we sample r and r' uniformly from a predefined interval; during inference, we fix both to a constant. See Tab. 3 for the specific values used in our experiments.

Component	BAIR	UCF-101	Kinetics-600
Architecture			
Temporal ViT (dim / layers / patch)	768 / 8 / 2	1024 / 16 / 2	1024 / 16 / 2
Canvas ViT (dim / layers / patch)	768 / 4 / 1	1024 / 8 / 1	1024 / 8 / 1
Spatial MAR (dim / layers / depth / patch)	768 / 8 / 2 / 1	1024 / 16 / 4 / 1	1024 / 16 / 4 / 1
Additional Architecture	Expert Layernorm [64]	Expert Layernorm [64]	MM-DiT [11]
Flow decoder (dim / layers)	1280 / 3	1280 / 3	1280 / 3
VAE model	Causal 3D CNN*	OmniTokenizer [56]	Non-causal 3D CNN [44]
MAR autoregressive steps [#]	4	8	10
Total parameters	211M	733M	733M
Training			
Batch size	192	64	192
Epochs	600	800	270
Resolution	17 × 64 × 64	17 × 256 × 256	17 × 128 × 128
Latent compression ratio	{1, 2} × 4 × 4	{1, 4} × 8 × 8	{1, 4} × 8 × 8
Latent resolution	9 × 16 × 16	5 × 32 × 32	5 × 16 × 16
Noise augmentation (r)	[0.2, 0.6]	[0.2, 0.6]	[0.2, 0.6]
Noise augmentation (r')	[0.0, 0.3]	[0.0, 0.3]	[0.0, 0.3]
Sampling			
Noise augmentation (r)	0.3	0.3	0.4
Noise augmentation (r')	0.2	0.2	0.2
Confidence temperature	6.5	6.5	6.5
Flow-head steps	30	30	30
Canvas CFG	1.5	1.5	2.25
Temporal CFG	1.2	1.2	1.1
Evaluation Resolution	16 × 64 × 64	16 × 256 × 256	16 × 64 × 64

Table 3: Model configurations for BAIR, UCF-101, and Kinetics-600. * Trained by ourselves with codebase of Song *et al.* [44]. # Otherwise specified, we use this step number for sampling.

B Next-Group Frame Prediction

For the next- K -frame prediction model, we slightly modify the architecture by appending K *canvas heads*, each implemented as a two-layer MLP, to the output of the Canvas ViT, as shown in Fig. 9. We also add lightweight temporal attention layers among spatial layers every four layers, following the decomposed attention design of Gupta *et al.* [17], to ensure temporal consistency. These canvas heads provide the spatial conditioning canvases for generating the next K frames within the Spatial MAR.

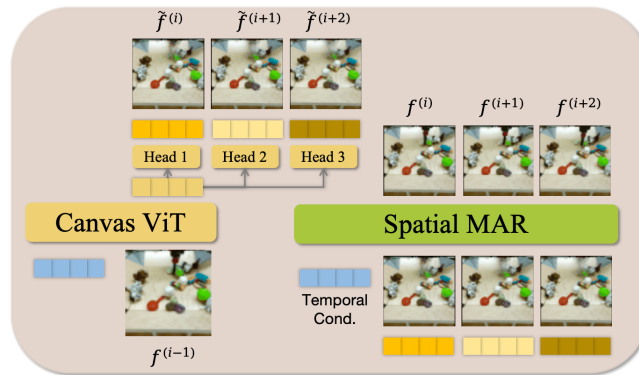


Fig. 9: Next-group frame prediction.